Regulating Cellular Behavior on Few-Layer Reduced Graphene Oxide Films with Well-Controlled Reduction States

Xuetao Shi, Haixin Chang, Song Chen, Chen Lai, Ali Khademhosseini, and Hongkai Wu**

Understanding the effect of graphene on cellular behavior is important for enabling a range of new biological and biomedical applications. However, due to the complexity of cell responses and graphene surface states, regulating cellular behaviors on graphene or its derivatives is still a great challenge. To address this challenge we have developed a novel, facile route to regulate the cellular behaviors on few-layer reduced graphene oxide (FRGO) films by controlling the reduction states of graphene oxide. Our results indicate that the surface oxygen content of FRGO has a strong influence on cellular behavior, with the best performance for cell attachment, proliferation and phenotype being obtained in moderately reduced FRGO. Cell performance decreased significantly as the FRGO was highly reduced. Moderate performance was found in non-reduced pure graphene oxide and control glass slides. Our results highlight the important role of surface physicochemical characteristics of graphene and its derivatives in their interactions with biocomponents, and may have great potential in enabling the utility of graphene based materials in various biomedical and bioelectronic applications.

1. Introduction

Graphene and its derivatives have been intensely studied for their unique electronic, mechanic, optoelectronic and photonic properties.[1–14] However, it has not been until recently that graphene is explored as a novel biocompatible nanomaterial for biosensing,[15–29] drug delivery,[30–32] and cell monitoring/growth.[15,33–40] In this regard, understanding the influence of graphene on cellular behavior is important for enabling a range of new biological and biomedical applications. Indeed, some studies have demonstrated the compatibility of cell growth on graphene. Graphene and its derivatives have been shown to possess an enhanced degree of cell adhesiveness and proliferation in chemical vapor deposition (CVD) grown graphene, chemically reduced graphene, and graphene based composites,[33–36] while being cytotoxic in some cases.[37–40] For example, a mechanically strong, electronically conductive graphene papers from filtration of chemically reduced graphene were developed as biocompatible substrates for cell growth.[33] CVD grown graphene also showed the promoted adherence of human osteoblast and mesenchymal stromal cells,[35] and enhanced the differentiation of neural stem cells into neurons.[36] On the other hand, graphene demonstrated a strong toxicity through accumulating on cell membranes, leading to apoptosis.[37] In general, the influence of graphene and its derivatives on cellular behaviors is still not clearly understood, and the key physicochemical characteristics in graphene based materials that influence cellular behaviors are not clear. Due to the complexity of cell responses and graphene surface states, it is challenging to elucidate or regulate cellular behavior on graphene and its derivatives.

Herein, to address this challenge, we have developed a novel, facile route to regulate the cellular behaviors on few-layer reduced graphene oxide (FRGO) films by controlling the reduction states of graphene oxide. The delicate tuning of the reduction states in FRGO was developed by a low-temperature thermal reduction method, which enabled controlling the oxygen contents in FRGO. FRGO films with three different reduction states were used to culture cells, and the cell adhesion, proliferation and phenotype behaviors on FRGO were investigated. The results indicate that the surface oxygenous content of FRGO has a significant influence on cellular behaviors with the best performance of cell adhesion, proliferation and phenotype being obtained in moderately reduced FRGO. Cell performance decreased significantly as the FRGO was highly reduced. Our results highlight the important role of surface physicochemical characteristics of graphene and its derivatives in their interactions with biocomponents, and may have great potential in enabling the utility of graphene based materials in various biomedical and bioelectronic applications.

Dr. X. T. Shi, Dr. H. X. Chang, Dr. S. Chen, Prof. A. Khademhosseini, Prof. H. K. Wu
WPI-Advanced Institute for Materials Research
Tohoku University
Sendai 980-8578, Japan
E-mail: hxchang@wpi-aimr.tohoku.ac.jp; chhkwu@ust.hk
Dr. C. Lai
Biomedical Engineering Research Center
Shenzhen Institution of Beijing University
Shenzhen 518057, China
Prof. H. K. Wu
Department of Chemistry
The Hong Kong University of Science and Technology
Hong Kong SAR

DOI: 10.1002/adfm.201102305

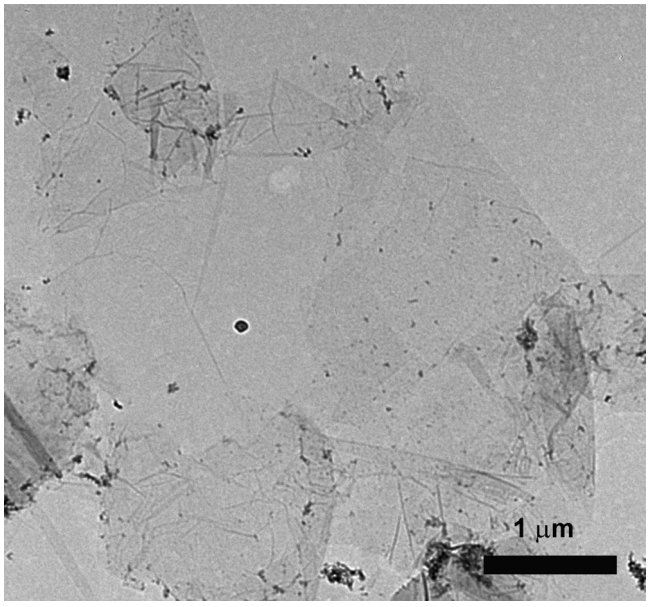

Figure 1. TEM image of single layer graphene oxide sheets.

2. Results and Discussion

2.1. Fabrication and Tuning Surface Property of FRGO Films

Single layer graphene oxide and few-layer graphene oxide films were prepared as described in the previous reports.[9–17] The single layer graphene oxide was characterized by transmission electron microscopy (TEM, **Figure 1**) and atomic force microscopy (AFM, **Figure 2**). Single layer graphene oxide was flexible, and had a number of observable wrinkles (Figure 1). The lateral size of single layer graphene oxide ranged from several hundreds of nanometers to several micrometers (Figure 1, Figure 2A) with the thickness of ~1 nm, typical for a single layer (Figure 2B).[9] We further studied the morphology of few-layer graphene oxide and few-layer reduced graphene oxide films on glass substrates. The pristine non-reduced few-layer graphene oxide (FRGO-0) film was continuous and usually had a thickness of ~7.5 nm (<8 layers) with an average roughness R_a of 3.2 nm (**Figures 3**A and 3B). For the 260 min reduced FRGO (FRGO-260) films, the thickness was ~6 nm with an average roughness R_a of 5.0 nm (Figure 3C). Therefore, there were no significant morphological differences in the few-layer graphene oxide and reduced FRGO films.

Interestingly the transparency of the FRGO films changed significantly as a result of thermal reduction and restoration of conjugated structures of graphene (Figure 3D).[9] FRGO-0 film was optically transparent, and became increasingly more opaque when reduced for a long period of time. The decreasing transparency in FRGO with reduction time is due to the loss of oxygen containing groups and the restoration of conjugated structures as indicated in the following X-ray photoelectron spectroscopy (XPS) measurements.

To further characterize the effect of the reduction on the FRGO films, we performed XPS measurements for more

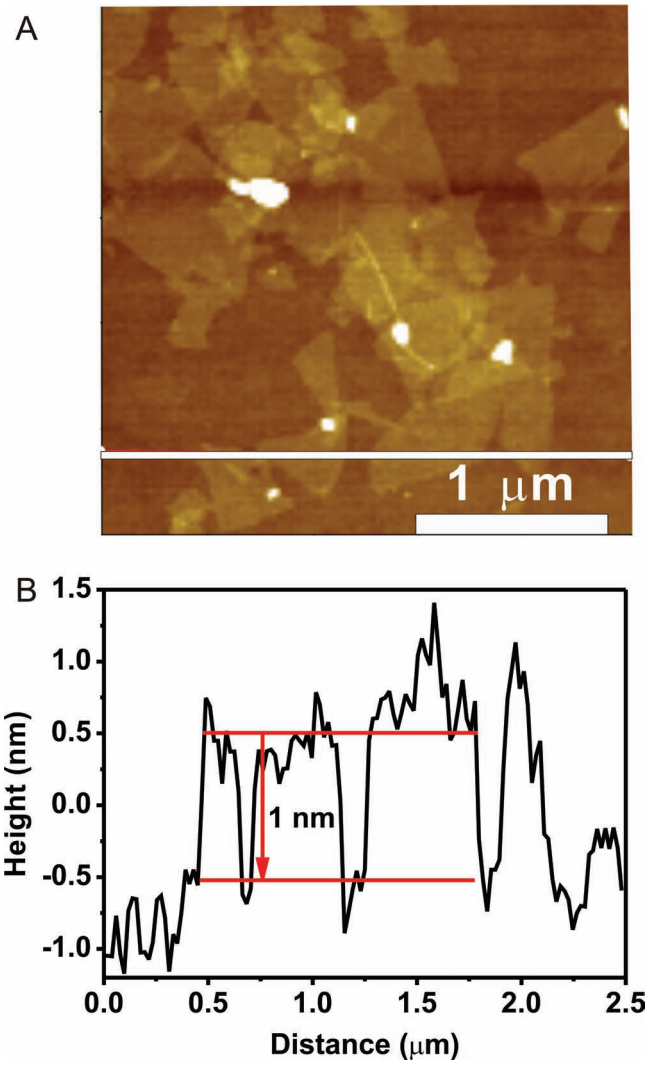

Figure 2. AFM image (A) and height profile (B, for white line in A) of single layer graphene oxide sheets.

information. XPS results showed that the content of oxygenous groups in the FRGO-0 and reduced FRGO films were vastly different. The oxygenous groups in graphene oxide are mainly carboxyl, hydroxyl, and epoxy groups, which are denoted as peaks and shoulders at the binding energy of ~287–288 eV (**Figure 4**) similar to previous reports.[9,41] The relative intensity of C-C component with peaks at ~284.5 eV increased with the reduction time, consistent with the darker color shown in digital images (Figure 3D). The O/C atomic ratios were ~0.6 for FRGO-0, and ~0.4 for 90 min reduced FRGO (FRGO-90), and ~0.3 for FRGO-260 (Figure 4), respectively. The loss of oxygenous groups was faster in the initial 90 min reduction, and became much slower in the following 170 min. The loss of the oxygen containing groups is due to the decomposition of oxygen containing groups in FRGO during the thermal reduction, and carbon dioxide (CO_2) and water (H_2O) will form during this decomposition. Therefore we can control the quantity of oxygen containing species in FRGO with the temperature and time of thermal reduction.

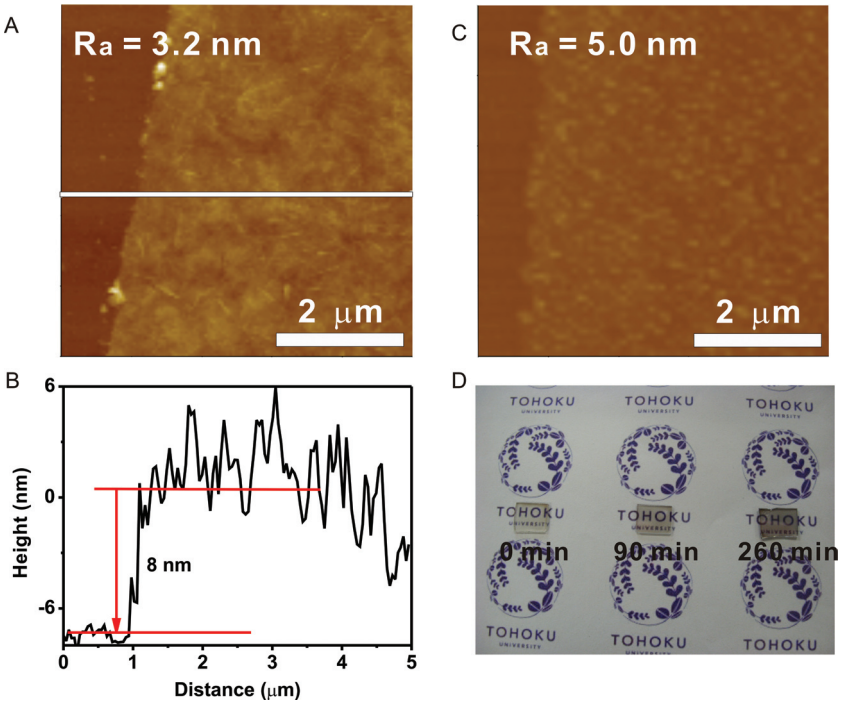

Figure 3. A) AFM image of non-reduced few-layer graphene oxide film on glass substrates. B) Height profile of the white line cross the film in (A). C) AFM image of 260 min reduced few-layer graphene oxide film. (D) Image of 0 min (left), 90 min (center) and 260 min (right) thermally reduced FRGO films at 150 °C.

To determine the changes in the hydrophobicity of the resulting films we also performed static water contact angle measurements. The water contact angles of pristine few-layer graphene oxide FRGO-0 and glass were measured to be 26.5 ± 7.3° (**Figure 5**B) and 36.0 ± 6.6° (Figure 5A), respectively. The water contact angle of FRGO-90 increased significantly to 60.4 ± 3.3°, indicating the obvious loss of oxygenous groups in the initial 90 min reduction (Figure 5C). Note that the contact angles of FRGO-90 and FRGO-260 (57.8 ± 2.5°) were not significantly different (Figures 5C and 5D), which may be explained by smaller differences in the oxygenous contents, and other parameters that influence water contact angles (e.g., hierarchical microstructures, wrinkles, etc.).[42]

2.2. Protein Adsorption on FRGO

Adsorbed proteins are critical for regulating cellular behaviors on materials surfaces such as adhesion and proliferation.[43–45] Therefore, the adsorption of individual proteins such as fibronectin and fibroblast growth factor (FGF), bovine serum albumin (BSA), as well as fetal bovine serum (FBS), which contains various serum proteins, was examined on different FRGO surfaces (**Figure 6**A). Quantitative measurements indicated that the amounts of adsorbed proteins such as FBS, fibronectin, and FGF on FRGO-90 was significantly higher than that on FRGO-260, FRGO-0 and the control glass slides. For example, the adsorbed fibronectin and FGF on FRGO-90 were ~3 folds higher than that on FRGO-260, and ~30% higher than that on FRGO-0, while these two proteins adsorbed on FRGO-0 similar to the controls (Figure 6A). Similar protein adsorption trend was observed in proteins from FBS. As for the adsorption of BSA, FRGO-260 exhibited ~3 folds lower protein adsorption than FRGO-90 and FRGO-0. In all 4 tested cases, FRGO-260 had much weaker protein adsorptions than FRGO-90 and FRGO-0.

The protein adsorption on materials surface is highly dependent on the surface physicochemical characteristics

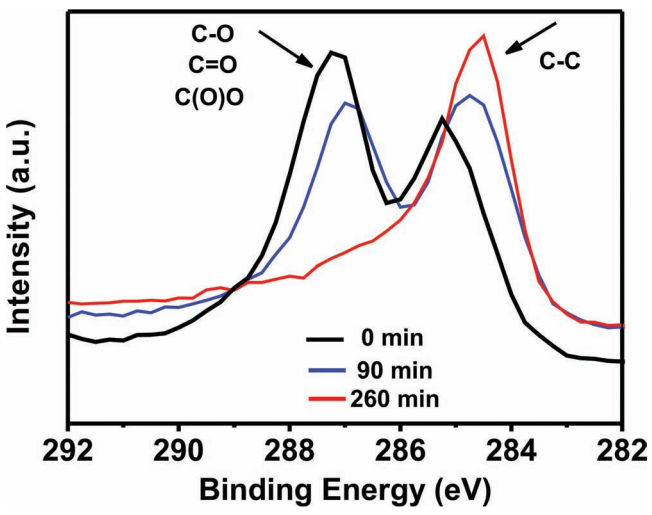

Figure 4. XPS spectra of 0 min, 90 min and 260 min thermally reduced FRGO films at 150 °C.

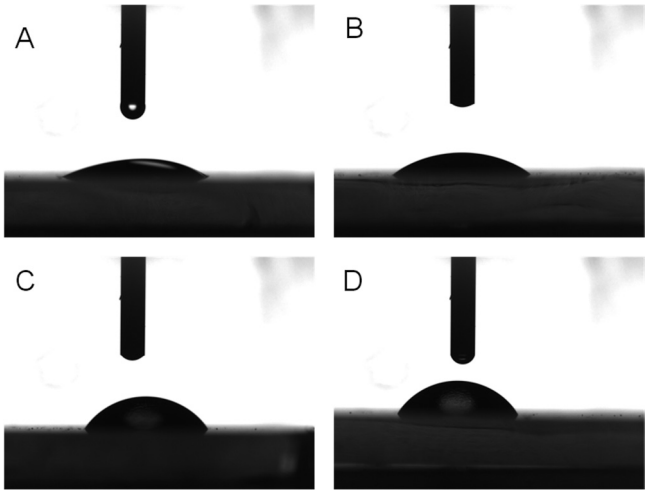

Figure 5. Water contact angles of the control glass (A, 36.0 ± 6.6°), and 0 (B, 26.5 ± 7.3°), 90 (C, 60.4 ± 3.3°), 260 (D, 57.8 ± 2.5°) min thermally reduced FRGO films on glass.

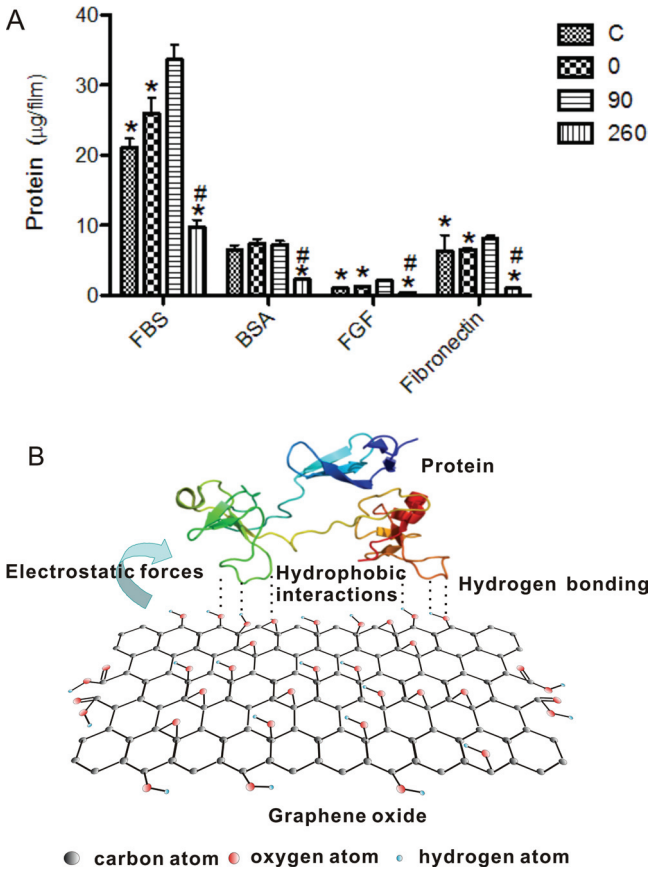

Figure 6. A) Adsorption of BSA, FGF, fibronectin and proteins from FBS on different FRGO surfaces. Pound sign (#) and asterisk (*) indicate statistical significance when compared with the control and FRGO-0, and with FRGO-90, respectively ($p < 0.05$). B) Scheme for main noncovalent interactions between graphene oxide and proteins, including electrostatic forces, hydrogen bonding, and hydrophobic interactions.

and noncovalent interactions (electrostatic forces, hydrogen bonding, hydrophobic interactions, etc.) induced by molecular structures of materials.[46–48] With increase of reduction time, FRGO has less oxygen containing groups and more conjugated carbon structures (Figure 4). The oxygenous groups in graphene oxide introduce charged and electronegative regions to the surfaces and enable the formation of hydrogen bonds with proteins, just like the interactions between small peptides and graphene oxide in our previous studies.[16] There are also possible hydrophobic interactions between proteins and FRGO.[47] Therefore, the possible reason for strongest adsorption in moderately reduced FRGO-90 may be due to a mixture of electrostatic forces, hydrogen bonding and hydrophobic interactions in FRGO to proteins (Figure 6B). For example, fibronectin protein has an isoelectric point of ~5.0 and is negatively charged in pH 7.2 buffer.[49] Although more oxygenous groups in FRGO-0 enhance the hydrogen bonding adsorption of fibronectin, they also induce more electrostatic repulsion to fibronectin from negative charges of oxygenous groups. However, in FRGO-260, both hydrogen bonding adsorption and electrostatic repulsion become weaker. As for hydrophobic interactions, their effects on protein adsorption on FRGO surfaces are unclear. FRGO-90 and FRGO-260 have similar hydrophobicity as indicated in similar water contact angles (Figures 5C and 5D). Therefore, the clear differences in protein adsorption in FRGO-90 and FRGO-260 should be induced more by the competition of electrostatic repulsion and hydrogen bonding. As for FRGO-0, it is much less hydrophobic than FRGO-90 and FRGO-260 (Figure 5B), and the hydrophobic interactions may play a more important role when comparing FRGO-0 with FRGO-90 and FRGO-260. In general, the result of competition of electrostatic repulsion, hydrogen bonding and hydrophobic interactions is that moderate oxygenous content FRGO-90 has the best performance on protein adsorption. It is well known that some specific extracellular matrix proteins such as fibronectin and vitronectin are highly important for cell adhesion onto the surface of biomaterials.[48,50,51] It is expected that such differences in protein adsorption (especially for fibronectin) will have a greater influence on the cellular behavior on FRGO as will be discussed later.

2.3. Cell Adhesion and Cell Proliferation on FRGO

To check the degree of cell adhesion and proliferation on FRGO films, various surfaces were seeded with myoblasts, osteoblasts, and fibroblasts and analyzed for their ability to induce cellular adhesion and proliferation. The attachment rates of different types of cells on different FRGO surfaces were compared to that of the control glass slide. The results of the cell attachment rates measurements revealed that more cells adhered to FRGO-90 in comparison to FRGO-260, FRGO-0 and the control samples (**Figure 7**A). Nearly 4 times more cells adhered on FRGO-90 after 3 h culture than that of FRGO-260. This difference was smaller at nearly 1.5 folds higher for FRGO-90 in comparison to cell adhesion on the control samples and dropped to 30-100% higher in comparison to FRGO-0. The differences in cell attachment rates may be attributed to adsorption levels of various proteins (e.g., fibronectin) adhesion on the different FRGO surfaces. It is known that fibronectin plays a positive role in cell adhesion, growth and migration.[50,51] In general, fibronectin can be adhered onto to the substrate from FBS or be deposited by adhering fibroblasts. Fibroblast secreted soluble compact fibronectin dimerized following by binding to $\alpha 5\ \beta\ 1$ integrin receptors on the surfaces of fibroblasts.[52] Fibronectin molecules form a complex, insoluble fibronectin matrix with the increasing concentration of integrin-bound fibronectin.[53] The fibronectin from these two originations was more effectively adsorbed on FRGO-90 than other substrates (Figure 6A), which may be the reason for the subsequent cell adhesive nature of this material.

The proliferations of the adherent myoblasts, osteoblasts, and fibroblasts on different FRGO surfaces were further investigated by a cell counting kit. As shown in Figure 7B, after 6 days of culture, a higher level of cell proliferation on FRGO-90 was observed compared to other FRGO surfaces. For example, cell numbers on FRGO-90 were ~30 folds higher than that on FRGO-260 for osteoblasts, fibroblasts, and ~3 folds higher for myoblasts, respectively. Cell numbers on FRGO-90 were also ~70% higher than that on FRGO-0 and the control for osteoblasts and myoblasts, and ~160% higher for fibroblasts,

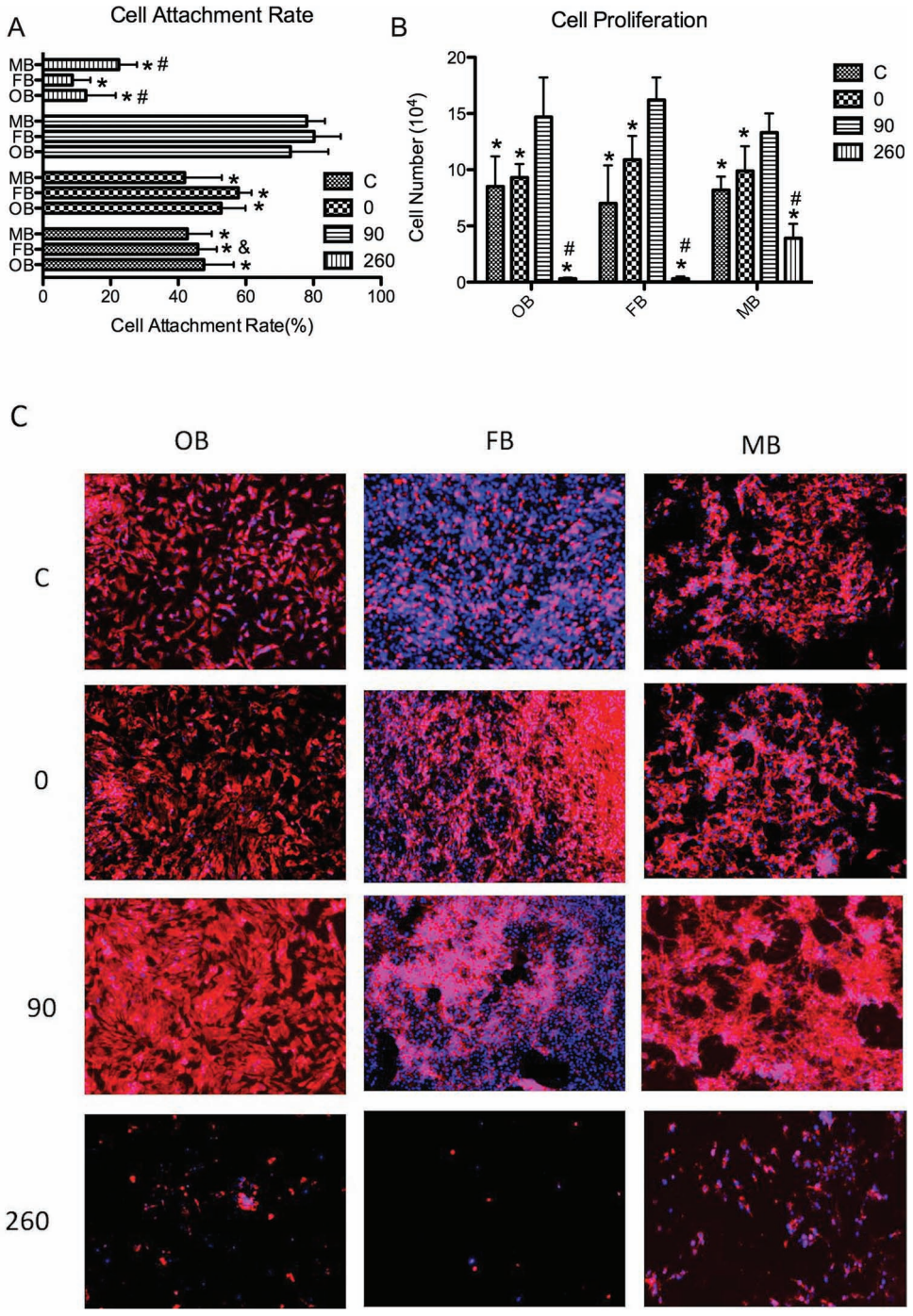

Figure 7. Cell attachment and proliferation. A) Cell attachment onto different FRGO films after 3 h of culture; B) Total cell numbers on different FRGO films after 6 days of culture with the initial seeded cell numbers of 1×10^4 for all films; and C) TRITC-phalloidin F-actin staining and DAPI cell nucleus staining, magnification: 4×. Pound (#), asterisk (*) and ampersand (&) sign indicate statistical significance when compared with the control and FRGO-0, with FRGO-90, and with FRGO-0, respectively ($p < 0.05$). OB, FB, and MB indicate osteoblasts, fibroblasts and myoblasts, respectively.

respectively. Cell numbers on FRGO-0 were comparable to that on the control, showing little enhancement effect on cell proliferation for untreated pristine graphene oxide compared with control glass. Therefore, cells on FRGO-90 had the highest level of proliferation, FRGO-260 had the weakest level of proliferation with the control and FRGO-0 substrates showing moderate levels of proliferation. Such differences in cell proliferation were more clearly demonstrated by TRITC-phalloidin F-actin staining and DAPI cell nucleus staining (Figure 7C). It should be noted that there was a remarkable decrease in cell numbers for all cell types on FRGO-260 cultured for 6 days indicating that it may not be a suitable long-term cell culture substrate.

We also note that our results are consistent with previously published reports that the chemically derived pristine graphene showed much worse cell performance compared with the pristine graphene functionalized with oxygen containing groups (–COOH), and the functionalized oxygen containing group on pristine graphene will help cell attachment and viability.[37]

The topography and physicochemical characteristics of material surfaces are the principal parameters for cell attachment and proliferation.[46,53,54] Electrostatic forces, hydrogen bonding, hydrophobic interactions and other forces between cells and material surface significantly influence the attachment process of cells on materials.[53] In this study, the topography of different FRGO surfaces was not significantly different, thereby the notable differences for cell attachment and proliferation on different FRGO surfaces are more likely induced by different surface physicochemical characteristics (e.g., content of surface oxygen groups) and the resulting differences in environmental proteins adsorption. Indeed, although FRGO-0 has more oxygen-containing groups, a moderately oxygenous FRGO-90 had the best performance in both cell attachment and proliferation for all the three different types of cells that were tested, while FRGO-260 with lowest oxygenous content had the worst performance. The result is consistent with the protein adsorption on FRGO. As mentioned above, proteins appeared to adsorb to highest degrees to FRGO-90 while the proteins did not adsorb significantly to FRGO-260 probably due to the differences in surface physicochemical characteristics and noncovalent interactions. Therefore, we speculate that the differences in environmental protein (e.g., fibronectin) adsorption on FRGO surface may induce the observed differences in cell attachment and proliferation.[48,50,51] Such oxygenous influence was also found in other materials systems such as in oxygen plasma-treated poly(N-isopropylacrylamide) (PNIPAAm) where oxygen groups on PNIPAAm promoted the proliferation of myoblasts.[55] These results strongly indicate that the amounts of oxygen-containing groups on material surface may regulate the resulting cell attachment and proliferation. Therefore, it may be possible to control cellular attachment and proliferation on graphene based materials by controlling the appropriate amount of oxygenous groups on the graphene surfaces.

2.4. Cell Phenotype on FRGO

The cell phenotype on different FRGO coated substrates was further studied to analyze the resulting cellular differentiation. First, the production of alkaline phosphatase (ALP) from osteoblasts was quantitatively determined after six days of culture (**Figure 8**A). The activity of ALP, an important enzyme widely found in bone tissue and an early marker for osteogenesis, was highest in osteoblasts cultured on FRGO-90 surface. The ALP activity from cells on FRGO-90 was ~8 folds higher than that on FRGO-260, 50% higher than that on FRGO-0, and 2 folds higher than that on control glass. The ALP activity performance

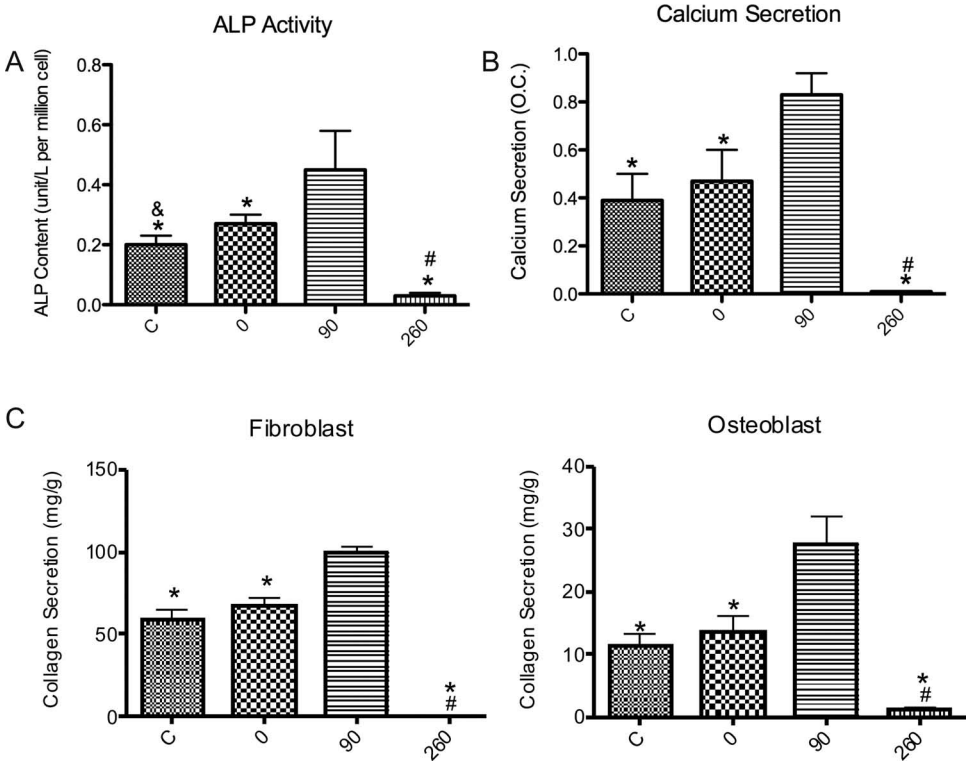

Figure 8. Cell phenotype on different FRGO surfaces. A) ALP activity of osteoblasts; B) Calcium secretion of osteoblasts; C) Collagen secretion of osteoblasts and fibroblasts. Pound (#), asterisk (*) and ampersand (&) sign indicate statistical significance when compared with the control and FRGO-0, with FRGO-90, and with FRGO-0, respectively ($p < 0.05$).

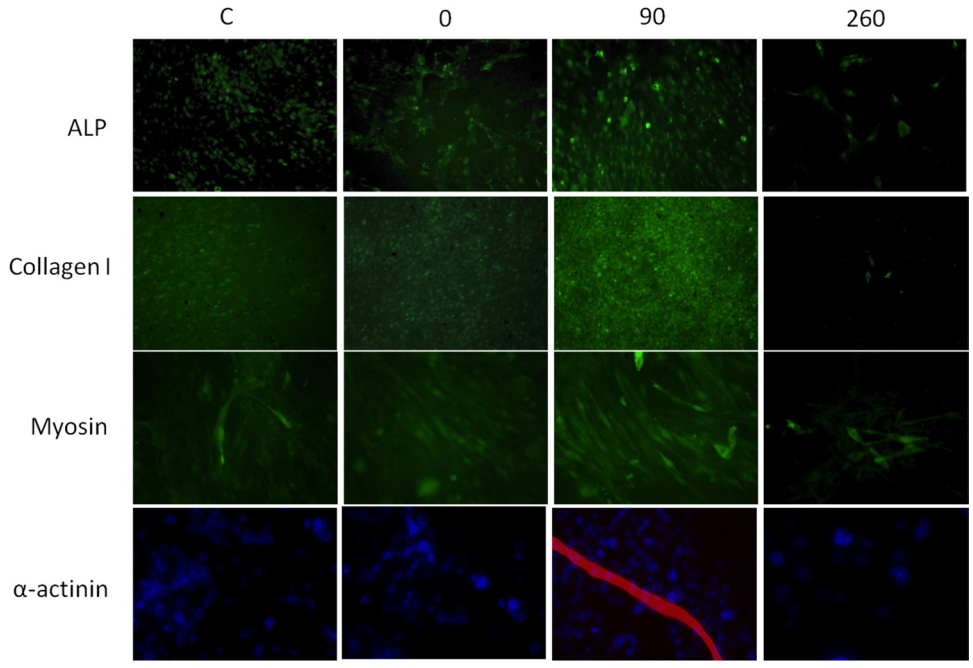

Figure 9. Immunofluorescent staining of type I collagen (osteoblasts and fibroblasts, green), and fast myosin heavy chain (green) and sarcomeric α-actinin (red) in the myotubes after 6 days of culture on control glass and different time reduced FRGO (0, 90, 260 min) films. OB: osteoblasts; FB: fibroblast. Magnification (Collagen): 4×; magnification (myosin and α- actinin): 10×.

was consistent with the results of cell attachment and proliferation on FRGO substrates.

The calcium deposition of osteoblasts and collagen secretion of both osteoblasts and fibroblast were also studied (Figures 8B and 8C) since they are important for biomineralized tissues such as bone.[56] After 6 days of culture, osteoblasts on FRGO-90 exhibited highest calcium secretion which was over 10 folds higher than that on FRGO-260, ~70% higher than that on FRGO-0, and ~2 folds higher than that on control glass (Figure 8B). Similar trends were also observed in the collagen secretion in both osteoblasts and fibroblast cells (Figure 8C). Immunofluorescent staining of type I collagen of osteoblasts and fibroblasts on different substrates is illustrated in **Figure 9**, which is also consistent with our previous analysis on cell attachment and proliferation. The results concur with the quantitative collagen assay, and suggest that osteoblasts and fibroblasts grow and proliferate more readily upon the surfaces of FRGO-90.

Cell phenotype of myoblasts was also investigated using a similar procedure (Figure 9). After myoblasts were attached on different substrates, horse serum was used to induce cellular differentiation. At day 6, immunofluorescence of two differentiation markers (myosin and α- actinin) were detected to evaluate the myogenic commitment. The results indicated myoblasts on FRGO-90 expressed more differentiation protein-myosin and fused into multinucleated myotubes. Although cells on FRGO-0 also expressed myosin, myotubes were not found on the surface of FRGO-0. Additionally, the controls and FRGO-260 showed only slight expression of myosin and no formation of myotubes. Therefore, FRGO-90 can also support and promote the differentiation commitment of myoblasts, which are quite different from FRGO-260, FRGO-0 and control.

3. Conclusion

We have shown that cellular behavior on FRGO films can be regulated by delicately tuning the reduction states of graphene oxide. The surface oxygen content of FRGO has a significant influence on cellular behaviors. Moreover, the moderately reduced FRGO has the best performance of cell attachment, proliferation and phenotype while highly reduced FRGO did not support cell adhesion and proliferation. We have also shown that the enhancement of cell adhesion and proliferation may be induced by enhanced extracellular matrix proteins adsorption in moderately reduced FRGO by non-covalent interactions. Therefore, the cellular behavior on graphene based materials may be regulated by tuning the surface chemistry of graphene. The results here envision the great potential of graphene with well controlled surface physicochemical characteristics in various biomedical and bioelectronic applications, considering the transparent, conductive, flexible/stretchable, and photothermal advantages of graphene.[57,58] These advantages of graphene could be more powerful in bioanalytical fields when combined with microfluidic technology.[27,59,60]

4. Experimental Section

Synthesis of Single Layer Graphene Oxide: Single layer graphene oxide was prepared similar to the previously published reports.[9–17] Briefly, graphite flakes (Alfa Aesar, USA) were pre-oxidized by concentrated H_2SO_4, $K_2S_2O_8$, and P_2O_5 by keeping the mixture at 80 °C for over 5 h. The mixture was then left to room temperature following by diluting with deionized (DI) water, filtering and washing thoroughly. The mixture was dried and re-oxidized by slowly adding H_2SO_4 and $KMnO_4$ under 0 °C with stirring. The mixture was then kept at 35 °C for ~2 h, and diluted

slowly using DI water. H_2O_2 was added to the obtained solution till the color changed into brilliant yellow. The solution was then filtered and washed by diluted HCl and DI water for several times. To remove the residue ions in the samples, the samples were dialyzed in DI water for over 1 week. The final product is called graphite oxide. Graphite oxide was sonicated for 1–2 h in DI water to be exfoliated to single layer graphene oxide.

Fabrication of Few-Layer Graphene Oxide Films: To prepare few-layer graphene oxide films, the single layer graphene oxide aqueous solution (~0.4 mg/mL) was spun or drop cast on glass slide. Typically, a 40 µl solution was used for a 1 cm × 1.2 cm glass slide. The glass slide was first covered by single layer graphene oxide aqueous solution, and was left to dry to obtain a homogenous, continuous few-layer graphene oxide film. The film was thermally reduced in air at 150 °C from 0–260 min, named few-layer reduced graphene oxide (FRGO).

Characterizations: TEM images of single layer graphene oxide were obtained by a JEM-2010 (JEOL) transmission electron microscope with 120 kV accelerated voltage. AFM images of single layer graphene oxide and FRGO were measured under tapping scanning modes (SPA-300HV or XE-100 scanning probes). The C1s XPS spectra of few-layer graphene oxide and reduced FRGO were collected by a PHI 1600 spectrometer. Water contact angles of FRGO films were measured by an OCA20 optical measuring system (Dataphysics, Germany).

Protein Adsorption: 1 mL 50 µg/mL fibronectin (in Tris-HCl buffer with 0.45 M NaCl and 12% glycerol, pH 7.2), 100 µg/mL bovine serum albumin (BSA, in pH 7.2 PBS buffer), 20 µg/mL FGF in DI water solution (pH 6.5–7.0), and FBS solution (pH 7.0–7.5) were added onto different FRGO surfaces and normal glass slides, respectively. After 3 h of incubation, FRGO films were rinsed with PBS and then the adsorbed proteins on FRGO surfaces were removed by 1% sodium dodecyl sulfate. The total protein was quantified using a QuantiPro bicinchoninic acid (BCA) assay kit (Sigma, USA).

Cell Culture, Seeding and Proliferation: Osteoblasts, fibroblasts, myoblasts were maintained in Eagle's medium (MEM) (for osteoblasts) and Dulbecco's modified eagle's medium (DMEM) (for fibroblasts and myoblasts) with 10% (v/v) fetal bovine serum (FBS) and 2% penicillin/streptomycin, respectively. Typically, 100 µL cell suspensions (1×10^6 cells/mL) were seeded onto the FRGO and normal glass slides in cell culture dish, and cultured for 6 days. After 6 h and 6 days of culture, Cell number was determined using cell counting kit-8 (Sigma-Aldrich, USA) following the manufacturer's instruction.

Osteogenesis Assay: Alkaline phosphatase (ALP) activity of osteoblasts was performed via pNPP assay (p-nitrophenyl phosphate liquid substrate, Sigma-Aldrich, USA).[53] Briefly, cells were pre-washed with PBS (pH = 7.2, Invitrogen, USA), and the cells growing on FRGO films were lysed in 0.1% Triton X-100 solutions for 10 min in 4 °C. After added pNPP into lysate, the mixed solution was incubated for 30 min at 37 °C, and the absorbance at 405 nm of the solution was measured by a plate reader. Finally, ALP activity was calculated via a formula offered by manufacturer after normalizing cell number. Quantification of mineralization was conducted according to previous report.[53] Briefly, osteoblasts on the films were washed with calcium and magnesium free PBS (Invitrogen, USA) and fixed in 10% (v/v) paraformaldehyde (Wako, Japan) for 10 min, and then washed with calcium and magnesium free PBS. 40 mM alizarin red solution (pH = 4.1) was added, and the films incubated at room temperature. After 30 min, the alizarin red solution was removed and the FRGO films were washed five times with calcium and magnesium free PBS. 10% acetic acid was added to remove the deposited alizarin red onto the films, and the films were then transferred to micro-centrifugation tube. The tube was then heated to 85 °C for 10 min and transferred on ice for 5 min. After centrifugation of the slurry in the tube, the supernatant was collected and neutralized with ammonium hydroxide. The absorbance values at 405 nm were determined with a plate reader. Calcium quantification was calculated from standard curve of calcium. Collagen content was measured via hydroxyproline quantification. Briefly, the cells on the film were digested and then added into a 4 M guanidine-HCl solution in 0.05 M sodium acetate. After centrifugation, the supernatant was discarded and then the residue was added into 5 mL 6 M HCl and 2 mL edible oil, and heated at 115 °C for 4 h. Afterwards, the residue was treated in chloramine-T solution, perchloric acid solution and paradime thylaminobenzaldehyde solution, respectively. The absorbance of the resulting solution at 560 nm was determined. Collagen quantification was calculated from standard curve of hydroxyproline.

Immunofluorescent and Actin Staining: After 6 days of culture, cells on the films were fixed in 4% paraformaldehyde solution for 10 min, and permeabilized in 0.3% Triton for 3 min. Thereafter, the specimens were incubated in goat blocking serum (Wako, Japan) for 1 h. Type I collagen secreted by osteoblasts and fibroblasts were detected with mouse monoclonal collagen I primary antibody as primary antibody and goat anti-mouse Alexa Fluor 488 (Invitrogen, USA) as the secondary antibody. Myosin was confirmed using mouse monoclonal IgG against fast skeletal myosin (Abcam, USA) as the primary antibody and goat anti-mouse Alexa Fluor 488 (Invitrogen, USA) as the secondary antibody. Sarcomeric α-actinin was monitored using mouse monoclonal anti-sarcomeric α-actinin as the primary antibody (Sigma, USA) and donkey anti-mouse antibody Alexa Fluor 594 (Invitrogen, USA) as secondary antibody. Nucleus was counterstained with DAPI (Invitrogen, USA) and F-actin was stained with TRITC-phalloidin. Briefly, after 6 days of culture, samples were washed in PBS and fixed with 1% paraformaldehyde for 10 min and 0.1% TritonX 100 (Sigma-Aldrich, USA) for 10 min. The samples were further washed with deionized water for 3 times following by staining with DAPI and TRITC-phalloidin for 30 min at 37 °C. Samples were again washed with deionized water for 3 times and viewed using fluorescent microscope (Zeiss, Germany).

Statistical analysis: Four experiments were performed for every assay and the results were expressed as means of ± standard deviations. Statistical significance was determined by analysis of variance with $P < 0.05$.

Acknowledgements

X.T.S. and H.X.C. contributed equally to this work. H.X.C., H.K.W., A.K., X.T.S., and S.C. acknowledge the support of WPI-Initiative funding from JSPS and MEXT, Japan. H.X.C. acknowledges the WPI-AIMR fusion research funding from JSPS and MEXT, Japan. The authors thank Prof. Z. J. Zheng in The Hong Kong Polytechnic University for the help in AFM measurements. C.L. thanks the funding from Science and Technology Research Foundation of Shenzhen Bureau of Science, Technology & Information (JC200903170498A).

Received: September 27, 2011
Revised: October 17, 2011
Published online: December 8, 2011

[1] A. K. Geim, K. S. Novoselov, *Nat. Mater.* **2007**, *6*, 183.
[2] Y. B. Zhang, Y. W. Tan, H. L. Stormer, P. Kim, *Nature* **2005**, *438*, 201.
[3] X. L. Li, X. R. Wang, L. Zhang, S. W. Lee, H. J. Dai, *Science* **2008**, *319*, 1229.
[4] S. Stankovich, D. A. Dikin, G. H. B. Dommett, K. M. Kohlhaas, E. J. Zimney, E. A. Stach, R. D. Piner, S. T. Nguyen, R. S. Ruoff, *Nature* **2006**, *442*, 282.
[5] X. Wang, L. Zhi, K. Müllen, *Nano Lett.* **2008**, *8*, 323.
[6] A. N. Cao, Z. Liu, S. S. Chu, M. H. Wu, Z. M. Ye, Z. W. Cai, Y. L. Chang, S. F. Wang, Q. H. Gong, Y. F. Liu, *Adv. Mater.* **2010**, *22*, 103.
[7] X. M. Geng, L. Niu, Z. Y. Xing, R. S. Song, G. T. Liu, M. T. Sun, G. S. Cheng, H. J. Zhong, Z. H. Liu, Z. J. Zhang, L. F. Sun, H. X. Xu, L. Lu, L. W. Liu, *Adv. Mater.* **2010**, *22*, 638.
[8] F. N. Xia, T. Mueller, Y. M. Lin, A. Valdes-Garcia, P. Avouris, *Nat. Nanotechnol.* **2009**, *4*, 839.

[9] H. X. Chang, Z. H. Sun, Q. H. Yuan, F. Ding, X. M. Tao, F. Yan, Z. J. Zheng, *Adv. Mater.* **2010**, *22*, 4872.
[10] H. X. Chang, G. F. Wang, A. Yang, X. M. Tao, X. Q. Liu, Y. D. Shen, Z. J. Zheng, *Adv. Funct. Mater.* **2010**, *20*, 2893.
[11] H. X. Chang, J. S. Cheng, X. Q. Liu, J. F. Gao, J. H. Li, X. M. Tao, F. Ding, Z. J. Zheng, *Chem. Euro. J.* **2011**, *17*, 8896.
[12] H. X. Chang, Z. H. Sun, K. Y. F. Ho, X. M. Tao, F. Yan, W. M. Kwok, Z. J. Zheng, *Nanoscale* **2011**, *3*, 258.
[13] H. X. Chang, X. J. Lv, H. Zhang, J. H. Li, *Electrochem. Commun.* **2010**, *12*, 483.
[14] J. L. Xia, F. Chen, J. H. Li, N. Tao, *Nat. Nanotechnol.* **2009**, *4*, 505.
[15] Y. Wang, Z. H. Li, D. H. Hu, C. T. Lin, J. H. Li, Y. H. Lin, *J. Am. Chem. Soc.* **2010**, *132*, 9274.
[16] Y. Wang, J. Lu, L. Tang, H. X. Chang, J. H. Li, *Anal. Chem.* **2009**, *81*, 9710.
[17] H. X. Chang, L. Tang, Y. Wang, J. H. Jiang, J. H. Li, *Anal. Chem.* **2010**, *82*, 2341.
[18] X. Dong, Y. Shi, W. Huang, P. Chen, L.-J. Li, *Adv. Mater.* **2010**, *22*, 1649.
[19] Y. J. Song, K. G. Qu, C. Zhao, J. S. Ren, X. G. Qu, *Adv. Mater.* **2010**, *22*, 2206.
[20] N. Mohanty, V. Berry, *Nano Lett.* **2008**, *8*, 4469.
[21] C.-H. Lu, H.-H. Yang, C.-L. Zhu, X. Chen, G.-N. Chen, *Angew. Chem. Int. Ed.* **2009**, *121*, 4879.
[22] S. Mao, G. H. Lu, K. H. Yu, Z. Bo, J. H. Chen, *Adv. Mater.* **2010**, *22*, 3521.
[23] H. B. Wang, Q. Zhang, X. Chu, T. T. Chen, J. Ge, R. Q. Yu, *Angew. Chem. Int. Ed.* **2011**, *50*, 7065.
[24] J. Balapanuru, J. X. Yang, S. Xiao, Q. L. Bao, M. Jahan, L. Polavarapu, J. Wei, Q. H. Xu, K. P. Loh, *Angew. Chem. Int. Ed.* **2010**, *49*, 6549.
[25] J. H. Jung, D. S. Cheon, F. Liu, K. B. Lee, T. S. Seo, *Angew. Chem. Int. Ed.* **2010**, *49*, 5708.
[26] H. Jang, Y. K. Kim, H. M. Kwon, W. S. Yeo, D. E. Kim, D. H. Min, *Angew. Chem. Int. Ed.* **2010**, *49*, 5703.
[27] Q. He, H. G. Sudibya, Z. Yin, S. Wu, H. Li, F. Boey, W. Huang, P. Chen, H. Zhang, *ACS Nano* **2010**, *4*, 3201.
[28] S. He, B. Song, D. Li, C. Zhu, W. Qi, Y. Wen, L. Wang, S. Song, H. Fang, C. Fan, *Adv. Funct. Mater.* **2010**, *20*, 453.
[29] C. X. Guo, X. T. Zheng, Z. S. Lu, X. W. Lou, C. M. Li, *Adv. Mater.* **2010**, *22*, 5164.
[30] Z. Liu, J. T. Robinson, X. M. Sun, H. J. Dai, *J. Am. Chem. Soc.* **2008**, *130*, 10876.
[31] L. M. Zhang, Z. X. Lu, Q. H. Zhao, J. Huang, H. Shen, Z. J. Zhang, *Small* **2011**, *7*, 460.
[32] H. Q. Bao, Y. Z. Pan, Y. Ping, N. G. Sahoo, T. F. Wu, L. Li, J. Li, L. H. Gan, *Small* **2011**, *7*, 1569.
[33] H. Chen, M. B. Muller, K. J. Gilmore, G. G. Wallace, D. Li, *Adv. Mater.* **2008**, *20*, 3557.
[34] S. Park, N. Mohanty, J. W. Suk, A. Nagaraja, J. H. An, R. D. Piner, W. W. Cai, D. R. Dreyer, V. Berry, R. S. Ruoff, *Adv. Mater.* **2010**, *22*, 1736.
[35] M. Kalbacova, A. Broz, J. Kong, M. Kalbac, *Carbon* **2010**, *48*, 4323.
[36] S. Y. Park, J. Park, S. H. Sim, M. G. Sung, K. S. Kim, B. H. Hong, S. Hong, *Adv. Mater.* **2011**, *23*, H263.
[37] A. Sasidharan, L. S. Panchakarla, P. Chandran, D. Menon, S. Nair, C. N. R. Rao, M. Koyakutty, *Nanoscale* **2011**, *3*, 2461.
[38] K. Wang, J. Ruan, H. Song, J. L. Zhang, Y. Wo, S. W. Guo, D. X. Cui, *Nanoscale Res. Lett.* **2011**, *6*, 8.
[39] K. H. Liao, Y. S. Lin, C. W. Macosko, C. L. Haynes, *Acs Appl. Mater. Interfaces* **2011**, *3*, 2607.
[40] W. B. Hu, C. Peng, M. Lv, X. M. Li, Y. J. Zhang, N. Chen, C. H. Fan, Q. Huang, *Acs Nano* **2011**, *5*, 3693.
[41] S. Stankovich, D. A. Dikin, R. D. Piner, K. A. Kohlhaas, A. Kleinhammes, Y. Jia, Y. Wu, S. T. Nguyen, R. S. Ruoff, *Carbon* **2007**, *45*, 1558.
[42] L. Feng, S. H. Li, Y. S. Li, H. J. Li, L. J. Zhang, J. Zhai, Y. L. Song, B. Q. Liu, L. Jiang, D. B. Zhu, *Adv. Mater.* **2002**, *14*, 1857.
[43] C. M. Wang, J. Bai, Y. H. Gong, F. Zhang, J. B. Shen, D. A. Wang, *Biotechnol. Prog.* **2008**, *24*, 1142.
[44] B. Geiger, *Nat. Rev. Mol. Cell Bio.* **2001**, *2*, 793.
[45] D. A. Wang, S. Varghese, B. Sharma, I. Strehin, S. Fermanian, J. Gorham, H. D. Fairbrother, *Nat. Mater.* **2007**, *6*, 385.
[46] R. J. Chen, Y. Zhang, D. Wang, H. J. Dai, *J. Am. Chem. Soc.* **2001**, *123*, 3838.
[47] J. Liu, S. Fu, B. Yuan, Y. Li, Z. X. Deng, *J. Am. Chem. Soc.* **2010**, *132*, 7279.
[48] T. Y. Chang, V. G. Yadav, S. D. Leo, A. Mohedas, B. Rajalingam, C.-L. Chen, S. Selvarasah, M. R. Dokmeci, A. Khademhosseini, *Langmuir* **2007**, *23*, 11718.
[49] D. F. Mosher, *Human Protein Data*(Ed.: A. Haeberli,), Wiley-VCH, Weinheim, Germany, **1998**.
[50] M. D. Pierschbacher, E. Ruoslahti, *Nature* **1984**, *309*, 30.
[51] S. K. Hanks, M. B. Calalb, M. C. Harper, S. K. Patel, *Proc. Natl. Acad. Sci.* **1992**, *89*, 8487.
[52] E. Ruoslahti, E. Engvall, E. G. Hayman, *Coll. Relat. Res.* **1981**, *1*, 95.
[53] X. T. Shi, Y. J. Wang, R. R. Varshney, L. Ren, F. Zhang, D. A. Wang, *Biomaterials* **2009**, *30*, 3996.
[54] O. Z. Fisher, A. Khademhosseini, R. Langer, N. A. Peppas. *Acc. Chem. Res.* **2010**, *43*, 419.
[55] K. Shimizu, H. Fujita, E. Nagamori, *Biotechnolog. Bioeng.* **2010**, *106*, 303.
[56] X. T. Shi, Y. J. Wang, L. Ren, Y. H. Gong, D. A. Wang, *Pharm. Res.* **2009**, *26*, 442.
[57] K. S. Kim, Y. Zhao, H. Jang, S. Y. Lee, J. M. Kim, K. S. Kim, J. H. Ahn, P. Kim, J. Y. Choi, B. H. Hong, *Nature* **2009**, *457*, 706.
[58] K. Yang, S. Zhang, G. Zhang, X. Sun, S.-T. Lee, Z. Liu, *Nano Lett.* **2010**, *10*, 3318.
[59] B. Huang, H. K. Wu, D. Bhaya, A. Grossman, S. Granier, B. K. Kobilka, R. N. Zare, *Science* **2007**, *315*, 81.
[60] K. N. Ren, W. Dai, J. H. Zhou, J. Su, H. K. Wu, *Proc. Natl. Acad. Sci. USA* **2011**, *108*, 8162.